

Mechanics of Hydraulic Fracturing

Experiment, Model, and Monitoring

Edited by Xi Zhang • Bisheng Wu
Diansen Yang • Andrew Bungler



WILEY

Mechanics of Hydraulic Fracturing

Mechanics of Hydraulic Fracturing

Experiment, Model, and Monitoring

Edited by

Xi Zhang
China University of Geosciences
Wuhan, China

Bisheng Wu
Tsinghua University
Beijing, China

Diansen Yang
Wuhan University
Wuhan, China

Andrew Bungler
University of Pittsburgh
Pittsburgh, PA, USA

WILEY

This edition first published 2023
© 2023 John Wiley & Sons, Inc.

All rights reserved. No part of this publication may be reproduced, stored in a retrieval system, or transmitted, in any form or by any means, electronic, mechanical, photocopying, recording or otherwise, except as permitted by law. Advice on how to obtain permission to reuse material from this title is available at <http://www.wiley.com/go/permissions>.

The right of Xi Zhang, Bisheng Wu, Diansen Yang, and Andrew Bungler to be identified as the editors for this work has been asserted in accordance with law.

Registered Office(s)

John Wiley & Sons, Inc., 111 River Street, Hoboken, NJ 07030, USA

Editorial Office

Boschstr. 12, 69469 Weinheim, Germany

For details of our global editorial offices, customer services, and more information about Wiley products visit us at www.wiley.com.

Wiley also publishes its books in a variety of electronic formats and by print-on-demand. Some content that appears in standard print versions of this book may not be available in other formats.

Limit of Liability/Disclaimer of Warranty

While the publisher and author have used their best efforts in preparing this book, they make no representations or warranties with respect to the accuracy or completeness of the contents of this book and specifically disclaim any implied warranties of merchantability or fitness for a particular purpose. No warranty may be created or extended by sales representatives or written sales materials. The advice and strategies contained herein may not be suitable for your situation. You should consult with a professional where appropriate. Further, readers should be aware that websites listed in this work may have changed or disappeared between when this work was written and when it is read. Neither the publisher nor authors shall be liable for any loss of profit or any other commercial damages, including but not limited to special, incidental, consequential, or other damages.

Library of Congress Cataloging-in-Publication Data

Names: Zhang, Xi (Geologist), editor.

Title: Mechanics of hydraulic fracturing : experiment, model, and monitoring / edited by Prof Xi Zhang, China University of Geosciences, Prof.

Bisheng Wu, Tsinghua University, Prof. Diansen Yang, Wuhan university, Prof. Andrew Bungler.

Description: First edition. | Hoboken, NJ, USA : Wiley, 2023. | Includes bibliographical references and index.

Identifiers: LCCN 2022030857 (print) | LCCN 2022030858 (ebook) | ISBN

9781119742340 (hardback) | ISBN 9781119742418 (adobe pdf) | ISBN

9781119742456 (epub) | ISBN 9781119742487 (oBook)

Subjects: LCSH: Hydraulic fracturing.

Classification: LCC TN871.255 .M43 2023 (print) | LCC TN871.255 (ebook) |

DDC 622/.3381-dc23/eng/20220907

LC record available at <https://lccn.loc.gov/2022030857>

LC ebook record available at <https://lccn.loc.gov/2022030858>

Cover Design: Wiley

Cover Image: © Studio One-One/Getty Images

Set in 9.5/12.5pt STIXTwoText by Straive, Pondicherry, India

Contents

	List of Contributors	<i>xiii</i>
	Foreword	<i>xv</i>
	Preface	<i>xvii</i>
1	Hydraulic Fracture Geometry from Mineback Mapping	1
	<i>R. G. Jeffrey</i>	
1.1	Introduction	1
1.2	Summary of Mapped Fracture Geometries	1
1.2.1	Fractures in Coal	1
1.2.1.1	DHM-7 Fracture	2
1.2.1.2	DDH 190 Fracture	2
1.2.2	Fractures in Hard Rock	5
1.2.2.1	Northparkes E48 Mapped Fractures	5
1.2.3	Other Mapped Fractures	7
1.3	Comparison of Mapped Fracture Geometries	7
1.3.1	Dimensionless Parameters	7
1.4	Fracture Geometry Summary	8
1.5	Conclusions	9
	References	9
2	Measurements of the Evolution of the Fluid Lag in Laboratory Hydraulic Fracture Experiments in Rocks	11
	<i>Dong Liu and Brice Lecampion</i>	
2.1	Introduction	11
2.2	Materials and Methods	12
2.2.1	Materials and Experimental Set-up	12
2.2.2	Methods	12
2.2.3	Experimental Design	13
2.3	Results	14
2.3.1	MARB-005 – A HF Growth with a Fluid Lag	14
2.3.2	MARB-007 – A HF Growth during and after the Injection	15
2.3.3	GABB-002 – A Point-Load Like HF Growth	16
2.4	Discussions and Conclusions	18
2.4.1	Resolution of the Fluid Front Location	18
2.4.2	Quasi-Brittle Effects	18
2.4.3	Hydraulic Fracture Surfaces	19
2.4.4	Conclusions	21
	Data Availability	21
	Appendix A Determination of the Time of Fracture Initiation	21
	References	22

3	Mapping Hydraulic Fracture Growth Using Tiltmeter Monitoring Technique	25
	<i>Z. R. Chen and R. G. Jeffrey</i>	
3.1	Introduction	25
3.2	Forward Problem Formulation	26
3.2.1	Forward Model Definition	26
3.2.2	Forward Model	27
3.2.2.1	Point Source Dislocation Singularity Model	28
3.2.2.2	A General Distributed Dislocation Model	29
3.3	Bayesian Inversion Method	30
3.4	Field Applications	31
3.4.1	Inversion Results Using the Point Source Forward Model	31
3.4.2	Inversion Results Using the General Planar Forward Model	31
3.5	Conclusions	34
	Acknowledgments	34
	References	34
4	Experimental Observations of Hydraulic Fracturing	37
	<i>Guangqing Zhang and Dawei Zhou</i>	
4.1	Introduction	37
4.2	Experimental Setup on Laboratory-Scale	37
4.3	Laboratory Investigation of Fluid-Driven Fractures in Various Applications	38
4.3.1	Hydraulic Fracturing in Oil and Gas Reservoirs	38
4.3.1.1	Basic Issues of Breakdown Pressure and Fracture Geometry	38
4.3.1.2	Multiple Hydraulic Fracture Growth	39
4.3.1.3	Interactions Between Hydraulic Fractures and Natural Fractures	40
4.3.1.4	Fracture Propagation Through the Layered Formation	41
4.3.1.5	Nonlinear Fracturing in the Deep Reservoir	42
4.3.1.6	Cyclic Fracturing	43
4.3.2	Environmental Fracturing in a Shallow Formation	44
4.3.3	Hydraulic Stimulation in EGS	44
4.4	Conclusions and Future Work	45
	References	46
5	First Field Trail and Experimental Studies on scCO₂ Fracturing	51
	<i>Haiyan Zhu, Lei Tao, Shouceng Tian, and Haizhu Wang</i>	
5.1	Introduction	51
5.2	Review on scCO ₂ Fracturing	52
5.2.1	Shale and scCO ₂ Interaction	52
5.2.1.1	Microscale Physical Changes	52
5.2.1.2	Microscale Chemical Changes	52
5.2.1.3	Macroscale Mechanical Changes	53
5.2.1.4	Conclusions on the Experiments on Shale and scCO ₂ Interaction	54
5.2.2	Experiments and Numerical Simulations on scCO ₂ Fracturing	54
5.2.2.1	Experiments on scCO ₂ Fracturing	54
5.2.2.2	Numerical Simulations on scCO ₂ Fracturing	57
5.3	A Field Trail on scCO ₂ Fracturing of Continental Shale in Yanchang Oil Field	57
5.3.1	scCO ₂ Fracturing Technology	57
5.3.2	scCO ₂ Fracturing Field Test	58
5.3.2.1	Reservoir Properties of Test Wells	58
5.3.2.2	Fracturing Process and Operation Parameters	58
5.3.3	Field Test Results and Analysis	59
5.3.3.1	Microseismic Monitoring and Inversion of Fracture Geometry	59

5.3.3.2	Production Data	60
5.4	Challenges in scCO ₂ Fracturing	60
5.4.1	scCO ₂ Fracturing Mechanism Is Still Not Clear	60
5.4.2	Challenges in Proppants Carrying	60
5.4.3	Challenge on the Predicting and Monitoring CO ₂ Phase	61
5.4.4	Lack of Specialized Equipment for scCO ₂ Fracturing	61
5.5	Conclusions	61
	Acknowledgments	61
	References	61
6	An Unstructured Moving Element Mesh for Hydraulic Fracture Modeling	65
	<i>John Napier and Emmanuel Detournay</i>	
6.1	Introduction	65
6.2	Discrete Model of a Planar Hydraulic Fracture	65
6.2.1	Unstructured Mesh	66
6.2.2	Discrete Elasticity Equation	66
6.2.3	Discretized Lubrication Equations for Channel Elements	67
6.2.4	Tip Elements	67
6.3	Time-Marching Algorithm	67
6.3.1	Iteration Loops	68
6.3.2	Local Front Update	68
6.3.3	Generation of a New Ring of Tip Elements	68
6.3.4	Crack Surface Remeshing	69
6.3.5	General Solution Algorithm Logic	69
6.4	Numerical Simulations: Stress Barriers	70
6.4.1	Description of Experiment	70
6.4.2	Numerical Simulations (no Remeshing)	70
6.4.3	Comparison with Experimental Results and Other Simulations	71
6.4.4	Illustration and Assessment of the Element Re-Meshing Strategy	71
6.5	Conclusions	73
	Acknowledgments	73
	References	73
7	Study of Hydraulic Fracture Interference with a Lattice Model	75
	<i>C. Detournay, B. Damjanac, M. Torres, and Y. Han</i>	
7.1	Introduction	75
7.2	XSite Code Overview	75
7.3	Numerical Studies of Fracture Interference	75
7.3.1	Interaction of a Hydraulic Fracture with a Natural Fracture	76
7.3.2	Interaction of Two Hydraulic Fractures	76
7.3.2.1	Numerical Study	76
7.3.2.2	Interpretation of Results	78
7.3.3	Interaction of Hydraulic Fractures in Injection of Multiple Clusters	79
7.3.4	Interaction of Hydraulic Fractures in Fractured Medium	81
7.3.5	Interaction of Hydraulic Fractures in Zipper-Stage Injection	83
7.4	Afterword	83
	References	85
8	The Tipping Point: How Tip Asymptotics Can Enhance Numerical Modeling of Hydraulic Fracture Evolution	87
	<i>A. Peirce</i>	
8.1	Introduction	87
8.2	Mathematical Model	87

8.2.1	Assumptions	87
8.2.2	Governing Equation	88
8.2.2.1	Elasticity	88
8.2.2.2	Fluid Transport	88
8.2.2.3	Boundary and Propagation Conditions	88
8.2.2.4	Tip Asymptotics, Vertex Solutions, and Generalized Asymptotes	89
8.3	Discretization, Coupled Equations, and the Multiscale ILSA Scheme to Locate the Free Boundary	91
8.3.1	Discretization	91
8.3.1.1	Displacement Discontinuity Formulation for Planar Fractures	91
8.3.2	Locating the Free Boundary Using the Implicit Level Set Algorithm (ILSA)	92
8.4	Numerical Results	95
8.4.1	Symmetric Stress Barrier: m -Vertex Solution vs Experiment and the Effect of Toughness	95
8.4.2	A Stress Drop: Distinct Propagation Regimes Along the Periphery	95
8.5	Conclusions	95
8.6	Acknowledgment	97
	References	97
9	Plasticity: A Mechanism for Hydraulic Fracture Height Containment	99
	<i>Panos Papanastasiou</i>	
9.1	Introduction	99
9.2	The Dependence of the Effective Fracture Toughness on Propagation Direction	100
9.3	Effective Fracture Toughness vs. Closure Stress	101
9.4	A New Brittleness Index Defines Fracture Containment	102
9.5	Conclusions	103
	Acknowledgments	104
	References	104
10	Turbulent Flow Effects on Propagation of Radial Hydraulic Fracture in Permeable Rock	107
	<i>E.A. Kanin, D.I. Garagash, and A.A. Osipov</i>	
10.1	Introduction	107
10.2	Model Formulation	108
10.2.1	Problem Definition	108
10.2.2	Governing Equations	109
10.2.2.1	Crack Elasticity	109
10.2.2.2	Fluid Flow	109
10.2.2.3	Fracture Propagation	110
10.2.2.4	Boundary Conditions	110
10.2.2.5	Global Fluid Volume Balance	110
10.3	Solution Approach	111
10.4	Solution Examples for Typical Field Applications	112
10.5	Limiting Propagation Regimes	115
10.6	Normalization of the Governing Equations	118
10.7	Problem Parameter Space Analyses	119
10.7.1	Zero Leak-Off Case (Impermeable Rock)	120
10.7.2	Nonzero Leak-Off Case (Permeable Rock)	121
10.8	Conclusions	122
	Acknowledgments	124
	References	125
11	Analysis of a Constant Height Hydraulic Fracture	127
	<i>E.V. Dontsov</i>	
11.1	Introduction	127

11.2	Governing Equations	128
11.3	Tip Region	129
11.4	Vertex Solutions	132
11.4.1	Storage Viscosity	132
11.4.2	Leak-off Viscosity	133
11.4.3	Storage Toughness	133
11.4.4	Leak-off Toughness	133
11.5	Full Solution	134
11.6	Application Examples	136
11.7	Summary	137
	References	137

12 Discrete Element Modeling of Hydraulic Fracturing 141

Mengli Li and Fengshou Zhang

12.1	Introduction	141
12.2	Discrete Element Modeling of Hydraulic Fracturing	142
12.3	Hydraulic Fracture Interacting with Natural Fractures	142
12.3.1	Hybrid Discrete-Continuum Method	143
12.3.2	Model Calibration for a Hydraulic Fracture in Intact Rock	144
12.3.3	Orthogonal Crossing	145
12.3.3.1	Effects of Stress Ratio and Friction of Natural Fractures	145
12.3.3.2	Effect of Strength (Toughness) Contrast	147
12.3.3.3	Effect of Stiffness (Modulus) Contrast	149
12.3.4	Non-Orthogonal Crossing	150
12.3.5	Fracturing Complexity	151
12.4	DEM Modeling of Supercritical Carbon Dioxide Fracturing	153
12.4.1	New Algorithm for the Toughness-Dominated Regime	153
12.4.2	Numerical Model Setup	154
12.4.2.1	Model Description	154
12.4.2.2	Model Verification	156
12.4.3	Hydraulic Fracturing in Intact Rock Sample	157
12.4.4	Hydraulic Fracturing in Fractured Rock Sample	161
12.5	DEM Modeling of Fluid Injection into Dense Granular Media	163
12.5.1	Background and Experimental Motivation	163
12.5.2	Model Setup	165
12.5.3	Effect of the Injection Rate	166
12.5.4	Dimensionless Time Scaling	168
12.5.5	Energy Partition	170
12.6	Discussion	171
12.7	Conclusions	171
	References	172

13 Interaction of a Hydraulic Fracture with Natural Fractures of Lesser Height and Weak Bedding Interfaces as a Possible Mechanism for Fracture Swarms 177

Xiaowei Weng and Olga Kresse

13.1	Introduction	177
13.2	Possible Mechanisms for Fracture Bifurcation	179
13.3	Interaction of Closely Spaced Parallel Fractures	182
13.3.1	Fracture Tip Extension in Overlapped Region	182
13.3.2	Instability of Closely Spaced Parallel Hydraulic Fractures – Shared Inlet	183
13.3.3	Instability of Closely Spaced Parallel Hydraulic Fractures – Separate Inlets	184
13.4	Possible Mechanisms for Creating Fracture Swarms	185

13.5	Conclusions	188
	References	189
14	Hydraulic Fracturing Mechanisms Leading to Self-Organization Within Dyke Swarms	193
	<i>Andrew. P. Bunger, D. Gunaydin, S. T. Thiele, and A. R. Cruden</i>	
14.1	Introduction	193
14.2	Swarm Morphology and Fundamental Drivers	193
14.3	Dyke Swarm Model and Energetics	194
14.4	Alignment	196
14.5	Avoidance	197
14.6	Stress Shadow	197
14.7	Stress Plugs	199
14.8	Attraction	199
14.9	Emergent Spacing	200
14.10	Simulating Dyke Swarm Assembly	201
14.11	Conclusions	202
	Acknowledgments	203
	References	203
15	Numerical Simulation of Thermal Fracturing During Heat Extraction from a Closed-Loop Circulation Enhanced Geothermal System	207
	<i>Z. Lei, Bisheng Wu, and Z. Chen</i>	
15.1	Introduction	207
15.2	Mathematical Formulation	208
15.2.1	Problem Description	208
15.2.2	Governing Equations of Coupled Thermoelastic Model	209
15.2.2.1	Fluid Flow	209
15.2.2.2	Rock Deformation	209
15.2.2.3	Fracture Initiation and Propagation	210
15.2.2.4	Thermal Transport Through Fluid Flow	211
15.2.2.5	Heat Transfer in Rock Matrix	211
15.2.3	Boundary and Initial Conditions	211
15.3	Solution Methodology and Computational Procedures	211
15.3.1	Coupled Fluid-Fracture Solver	211
15.3.1.1	Weak Form and FEM Discretization	211
15.3.1.2	Extended Finite Element Approximation	212
15.3.2	Coupled Fluid-Thermal Solver	213
15.3.3	Solution Strategy	213
15.4	Numerical Results	214
15.4.1	Fluid Flow and Production Temperature	214
15.4.2	Temperature Distribution in Rock Formation	216
15.4.3	Fracture Propagation	216
15.4.3.1	Single Fracture Case	216
15.4.3.2	Double Fracture Case	220
15.5	Conclusions	221
	References	221
16	Multiple Hydraulic Fractures Growth from a Highly Deviated Well: A XFEM Study	225
	<i>Yun Zhou and Diansen Yang</i>	
16.1	Introduction	225
16.2	Problem Formulation	227
16.2.1	Governing Equations	228

16.2.1.1	Solid Deformation	228
16.2.1.2	Fluid Flow in Matrix	229
16.2.1.3	Fluid Flow in Fractures	229
16.2.1.4	Flow Rate Division to Multiple Fractures	229
16.2.1.5	Fracture Propagation	229
16.2.2	Weak Forms	230
16.3	Numerical Method	230
16.3.1	XFEM Approximation of $u(x, t)$ and $p(x, t)$	230
16.3.2	Spatial and Time Discretization	231
16.3.3	Solution Strategy	231
16.3.3.1	Solution of HM-Coupled Equations	231
16.3.3.2	Solution of Flow Rate Division	231
16.4	Numerical Results	232
16.4.1	Verification of the Model	232
16.4.2	Multi-Cluster Hydraulic Fracturing in High-Angle Well	233
16.4.2.1	Model Set-up	234
16.4.2.2	Operational Parameters	235
16.4.2.3	Deviation Angle	236
16.4.2.4	Fracture Spacing	239
16.4.2.5	Fracture Placement	240
16.4.2.6	Fracture Number	241
16.5	Discussion	245
16.6	Conclusions	245
	Appendix 16.A Dimensionless Toughness κ	245
	Appendix 16.B Dimensionless Parameter Γm	246
	Appendix 16.C Dimensionless Variability Coefficient C_v	246
	References	246

17 Hydraulic Fracturing-Induced Slip on a Permeable Fault 251

Xi. Zhang, R. G. Jeffrey, and J. Yang

17.1	Introduction	251
17.2	Model Setup	252
17.3	Summary of Modeling Results	254
17.3.1	Fully Closed Fractures	254
17.3.1.1	Constant Fault Permeability	254
17.3.1.2	Enhanced Fault Permeability	254
17.3.1.3	Fault Permeability Reduction	255
17.3.2	Partially Opened Fracture	256
17.3.2.1	Planar Fault	256
17.3.2.2	Nonplanar Fault	256
17.4	Radiated Energy	256
17.5	Conclusions and Future Work	258
	Acknowledgment	259
	References	259

Index 263

List of Contributors

Andrew P. Bunger

Department of Civil and Environmental Engineering,
University of Pittsburgh, Pittsburgh, PA, USA
and

Department of Chemical and Petroleum Engineering,
University of Pittsburgh, Pittsburgh, PA, USA

Z. R. Chen

CSIRO Energy, Clayton South, Victoria, Australia

A. R. Cruden

School of Earth Atmosphere & Environment, Monash
University, Clayton, Victoria, Australia

B. Damjanac

Itasca Consulting Group, Minneapolis, MN, USA

Emmanuel Detournay

Department of Civil, Environmental, and
Geo-Engineering, University of Minnesota, Minneapolis,
MN, USA

C. Detournay

Itasca Consulting Group, Minneapolis, MN, USA

E. V. Dontsov

ResFrac Corporation, 555 Bryant St.,
#185 Palo Alto, CA, USA

D. I. Garagash

Department of Civil and Resource Engineering,
Dalhousie University,
Halifax, Nova Scotia, Canada

D. Gunaydin

Department of Civil and Environmental Engineering,
University of Pittsburgh, Pittsburgh, PA, USA

Y. Han

Aramco Services Company: Aramco Research Center,
Houston, TX, USA

R. G. Jeffrey

SCT Operations Pty. Ltd., Wollongong, New South Wales,
Australia

E. A. Kanin

Project Center for Energy Transition and ESG,
Skolkovo Institute of Science and Technology (Skoltech),
Moscow, Russian Federation

Olga Kresse

Schlumberger, Houston, TX, USA

Brice Lecampion

Geo-Energy Laboratory, Gaznat Chair on Geo-Energy,
Ecole Polytechnique Fédérale de Lausanne, EPFL-ENAC-
IIC-GEL, Lausanne, Switzerland

Z. Lei

Department of Hydraulic Engineering, Tsinghua
University, Haidian, Beijing, China

Mengli Li

Key Laboratory of Geotechnical and Underground
Engineering of Ministry of Education, Tongji University,
Shanghai, China

and

Department of Geotechnical Engineering, College of Civil
Engineering, Tongji University, Shanghai, China

Dong Liu

Geo-Energy Laboratory, Gaznat Chair on Geo-Energy,
Ecole Polytechnique Fédérale de Lausanne, EPFL-ENAC-
IIC-GEL, Lausanne, Switzerland

John Napier

Department of Mining Engineering,
University of Pretoria,
Hatfield, Pretoria
South Africa

A. A. Osiptsov

Project Center for Energy Transition and ESG,
Skolkovo Institute of Science and Technology (Skoltech),
Moscow, Russian Federation

Panos Papanastasiou

Department of Civil and Environmental Engineering,
University of Cyprus, Nicosia, Cyprus

A. Peirce

Department of Mathematics, University of British
Columbia, Vancouver, British Columbia, Canada

Lei Tao

State Key Laboratory of Oil and Gas Reservoir Geology and
Exploitation, Chengdu University of Technology,
Chengdu, China

S. T. Thiele

Helmholtz Institute Freiberg for Resource Technology,
Helmholtz-Zentrum Dresden-Rossendorf, Freiberg,
Germany

Shouceng Tian

State Key Laboratory of Petroleum Resources and
Prospecting, University of Petroleum (Beijing),
Beijing, China

M. Torres

Itasca Consulting Group, Minneapolis, MN, USA

Haizhu Wang

State Key Laboratory of Petroleum Resources and
Prospecting, University of Petroleum (Beijing),
Beijing, China

Xiaowei Weng

Retired, Schlumberger, Houston, TX, USA

Bisheng Wu

Department of Hydraulic Engineering, Tsinghua
University, Beijing, China

Diansen Yang

School of Civil Engineering, Wuhan University,
Wuhan, China

J. Yang

Institute of Rock and Soil Mechanics, Chinese Academy of
Sciences, Wuhan, China

Xi Zhang

Faculty of Engineering, China University of Geosciences,
Wuhan, China
and
SCT Operations Pty Ltd, Wollongong, Australia

Fengshou Zhang

Key Laboratory of Geotechnical and Underground
Engineering of Ministry of Education, Tongji University,
Shanghai, China

and

Department of Geotechnical Engineering, College of Civil
Engineering, Tongji University, Shanghai, China

Guangqing Zhang

College of Petroleum Engineering, China University of
Petroleum-Beijing, Beijing, China

Yun Zhou

State Key Laboratory of Geomechanics and Geotechnical
Engineering, Institute of Rock and Soil Mechanics, Chinese
Academy of Sciences, Wuhan, Hubei, China

Dawei Zhou

College of Petroleum Engineering, China University of
Petroleum-Beijing, Beijing, China

Haiyan Zhu

State Key Laboratory of Oil and Gas Reservoir Geology and
Exploitation, Chengdu University of Technology,
Chengdu, China

Foreword

For about 15 years until his retirement from the Commonwealth Scientific and Industrial Research Organization (CSIRO) in 2015, Rob Jeffrey led a group of scientists, technical officers, students, and academic visitors, all engaged in hydraulic fracturing research. Under Rob's direction, the CSIRO Hydraulic Fracturing (CSIRO HF) group, located in Melbourne, was a vibrant center, unique in the diversity of its activities that involved field testing, laboratory experiments, theoretical modeling, and numerical simulations. Many authors of this book have been associated with the CSIRO HF group, and their contributions are tributes to Rob's inspired leadership.

A permanent focus of the CSIRO HF group was to support the development of hydraulic fracturing as a means to precondition a rock mass for cave inducement of ore bodies and coal mine goafs. This application of hydraulic fracturing to mining was Rob's brainchild, an invention foreshadowed by the experience and expertise Rob gained in the United States while working, first, for the mining industry and later for the petroleum industry in research and development. His patented technique is now being used routinely in mines in several countries, including Australia, Chile, and Indonesia. Preconditioning by hydraulic fracturing has a profound economic impact on hard rock mines relying on block caving and on longwall coal mines, in some cases ensuring the economic viability of these operations.

One of Rob's outstanding achievements at CSIRO was the establishment of a world-class laboratory dedicated to

hydraulic fracturing research with a large polyaxial cell as its centerpiece. A particular point of pride for Rob was the heavy-duty equipment used to conduct field tests. The lab was the birthplace of innovative experiments; some were conducted in glass or polymethyl methacrylate (PMMA) to enable visualization of the fracture evolution and photometric measurements of the aperture field to test computational models, while others explored the interaction of a hydraulic fracture with discontinuities or with a free surface, to cite a few. Although experiments in the field or in the lab are Rob's passion, he was always enthusiastically supportive of theoretical and computational work.

Some members of the former CSIRO HF group have moved to academic positions in China, Europe, and North America, but they remain engaged in hydraulic fracturing research. With this migration, the theoretical expertise and know-how for innovative experimental work gained in the CSIRO lab has been kept alive and further flourished. This is one of Rob's enduring legacies.

On a personal note, I am indebted to Rob for giving me the wonderful opportunity to work in his group. It was initiated at the ARMA Vail Symposium in 1999, when Rob asked me "would you be interested to spend some of your sabbatical in Melbourne" This led to a long-term collaboration and a chance to discover Australia on multiple occasions.

Emmanuel Detournay, University of Minnesota,
Minneapolis, USA

Preface

This volume of contributed chapters comes from the network of researchers working on mechanics of hydraulic fracturing in theory, experiments, and applications. Many of these contributors comprised the participants in a series of Hydraulic Fracturing Summits held from 2001 to 2015. These workshops provided a venue for lively debates and effective exchanges of ideas. The success of these Summits is attributed to Rob Jeffrey and Emmanuel Detournay, who initiated this series of annual meetings and fostered the community in their collaborations. They recognized the scientific significance of this fast-growing field prior to the surge of unconventional oil and gas reservoir stimulation, and through this workshop mentored a generation of hydraulic fracturing researchers.

This volume is devoted to celebrating the 70th birthday of Rob Jeffrey, who was the program leader at Commonwealth Scientific and Industrial Research Organisation (CSIRO), Australia, when three of the editors worked there. Rob is one of the pioneers for the application of hydraulic fracturing in coal seam gas reservoir stimulation and the foundation of the knowledge on hydraulic fracture growth in naturally fractured rocks. During his forty years working in hydraulic fracturing field, he launched many important research directions, being among the first to work in areas such as fracture network formation, novel fracture monitoring methods, mine-through mapping of full-scale hydraulic fractures, and use of hydraulic fracturing to modify rock mass properties for both block caving and longwall coal mining. All of his work brought together theoretical and experimental methods in order to address new issues with rigor and pragmatism. In recognition of Rob's outstanding contributions both to the field and to their careers, his Hydraulic Fracturing Summit colleagues and others are happy to contribute this book that is in his honor.

This volume contains 17 chapters, covering a wide range of relevant research topics and important application areas. The editors wish to thank every contributor for their diligence and careful choice of topics. The chapters will provide the first comprehensive story on these experimental and field monitoring results, including comparisons of several numerical methods with industrial applications. This book will benefit a wide spectrum of readers, ranging from newcomers seeking an efficient orientation to the field to seasoned experts looking for a unique set of references on some of the most important issues within the hydraulic fracturing community over the past two decades.

The editors are grateful to those anonymous reviewers of the book proposal for their positive comments and constructive suggestions and to the many volunteer reviewers who spent tremendous amount of time and effort in the evaluation of each chapter. We also owe much to Dr. Ritu-parna Bose, Layla Harden, and Stefanie Volk at Wiley, who are aware of the rapid-growing knowledge and social impact of hydraulic fracturing, and along with other editorial team members supporting this book. Without their vision, enthusiasm, and diligent efforts, this book would not have been possible.

Xi Zhang, China University of Geosciences,
Wuhan, China
Bisheng Wu, Tsinghua University,
Beijing, China
Diansen Yang, Wuhan University,
Wuhan, China
Andrew Bunger, University of Pittsburgh,
Pittsburgh, PA, USA

1

Hydraulic Fracture Geometry from Mineback Mapping

R. G. Jeffrey

SCT Operations Pty. Ltd., Wollongong, New South Wales, Australia

KEY POINTS

- Details of full-size hydraulic fracture geometry are only available from mapping of mined fractures.
- Hydraulic fractures mapped in naturally fractured coal, sandstone, and in crystalline rock show many similarities that result from interactions with natural fractures and shear structures.

1.1 Introduction

Hydraulic fractures have been mapped during mining in a range of rock types and in a variety of geologic and in situ stress settings. Mapping has occurred for fractures placed into clay and soil [1], welded tuff [2], coal ([3–5]), andesite [6], and other crystalline and metamorphic rocks in porphyry ore bodies [7–9].

Coal seams are typically fractured for the purpose of stimulating production of seam gas (coalbed methane), either for commercial use of the gas or to improve drainage of gas from the coal before mining. Approximately 50 hydraulic fractures have been mined and mapped in detail in coal seams in the United States and Australia ([3, 4, 10, 11]; Jeffrey et al. 1993). In comparison, fractures mapped in other materials (soil and rock) total less than 20, with 10 of these located in porphyry copper and gold orebodies ([6, 7, 9]; containing intrusive monzonites and metamorphosed volcanic sediments. These fractures were placed as part of investigations into fracture geometry expected to be produced by hydraulic fractures used to precondition the orebody in advance of mining. The fractures placed into welded tuff were part of early research into hydraulic fracture growth [2] and the soil fractures were part of a study of fracturing for waste remediation [1].

By comparing the fracture geometry mapped in these different natural materials, common and disparate features of the fractures are highlighted. To help with the comparison,

dimensionless groups that have been shown to be important in hydraulic fracture growth are calculated or estimated for each mapped fracture. There is an extensive body of work using experimental, analytical, and numerical methods to investigate interactions of hydraulic fractures with bedding and natural fractures and faults. This paper limits itself to the mapped geometry exposed by mining of full-size hydraulic fractures and presents a comparison of features found in coal, sandstone, and stronger metamorphic or igneous rocks.

1.2 Summary of Mapped Fracture Geometries

Selected hydraulic fractures that were placed in coal, sandstone, and hard rock are described in this section. For each fracture the treatment parameters, rock properties, and in situ properties are listed.

1.2.1 Fractures in Coal

Two fractures placed into coal seams will be described, one located in Australia as described by Jeffrey et al. (1993) and one located in the United States [10]. The fracture descriptions include details of the treatment and site characterization, including rock mechanical properties and in situ stress data.

1.2.1.1 DHM-7 Fracture

As part of a program to better understand hydraulic fracture stimulation of coal, well DHM-7 was fractured using linear gel with sand proppant [10]. DHM-7 was drilled and completed open hole through the Blue Creek coal seam in Alabama. The well was located over the Oak Grove Mine in the Warrior Basin. Table 1.1 summarizes the parameters of the site and the treatment parameters. It is difficult to measure σ_H in coal because the cleat and natural fractures make overcoring impractical and the determination of fracture initiation is difficult when using a microfrac stress test. A value for σ_H that is larger than the vertical stress has been selected because the mine back mapping revealed no development of propped fractures at right angles to the direction of the main vertical fracture branch.

Room and pillar mining exposed the fracture in the coal rib around the sides of two pillars and along the coal rib nearest the well (Figure 1.1). A vertical and horizontal propped fracture (T-shaped) was found with the vertical part consisting of a number of parallel strands. The vertical fracture extended for more than 30 m to the north of the well. A horizontal propped fracture, extending over the vertical fracture, was located at the coal-roof rock interface and was mapped in detail (see Figure 1.2). The fracture was not mined to the south, but based on the area and fracture widths mapped, the propped fracture mapped on the north side of well DHM-7 was estimated to contain approximately 75% of the sand proppant injected [12].

The treatment pumped into DHM-7 used a non-crosslinked guar-based gel fluid that was injected at an average rate of 8.3 barrels/min (0.022 m³/s). A thick resin-coated sand system was pushed into the near-well part of the

fracture on the morning following the main treatment. This resin coated sand was used to test its ability to stabilize the wellbore region. It is designed to retain 80% of the sand's permeability after curing. Much of the vertical fracture exposed nearest the wellbore, at location A in Figure 1.1, was filled with this resin-coated sand. Samples of this propped fracture were excavated and taken from the mine for later analysis and display. No resin-coated sand was found at the next exposure at location B. Mapping of the horizontal fracture was done at the detail level represented in Figure 1.2 along all propped exposures.

The mapped geometry in DHM-7 and other cases presented below rely on the proppant to mark the fracture path. The hydraulic fracture typically extends beyond the proppant, especially when less viscous fluids are used. Hydraulic fractures cannot in general be found or mapped if they do not contain proppant. The distribution of the proppant, especially in a horizontal fracture, depends on both the fracture width and the fluid velocity field. Proppant transport in horizontal fractures is an area of study that has received little attention, primarily because horizontal fracture growth is thought to be a rare occurrence at depths greater than approximately 300 m. The hydraulic fractures described below that were placed into the orebody at Northparkes at a depth of 580 m were horizontal. T-shaped fractures are common in stimulation of coal and better models that can deal with horizontal fracture growth and the associated proppant transport problem would be welcome.

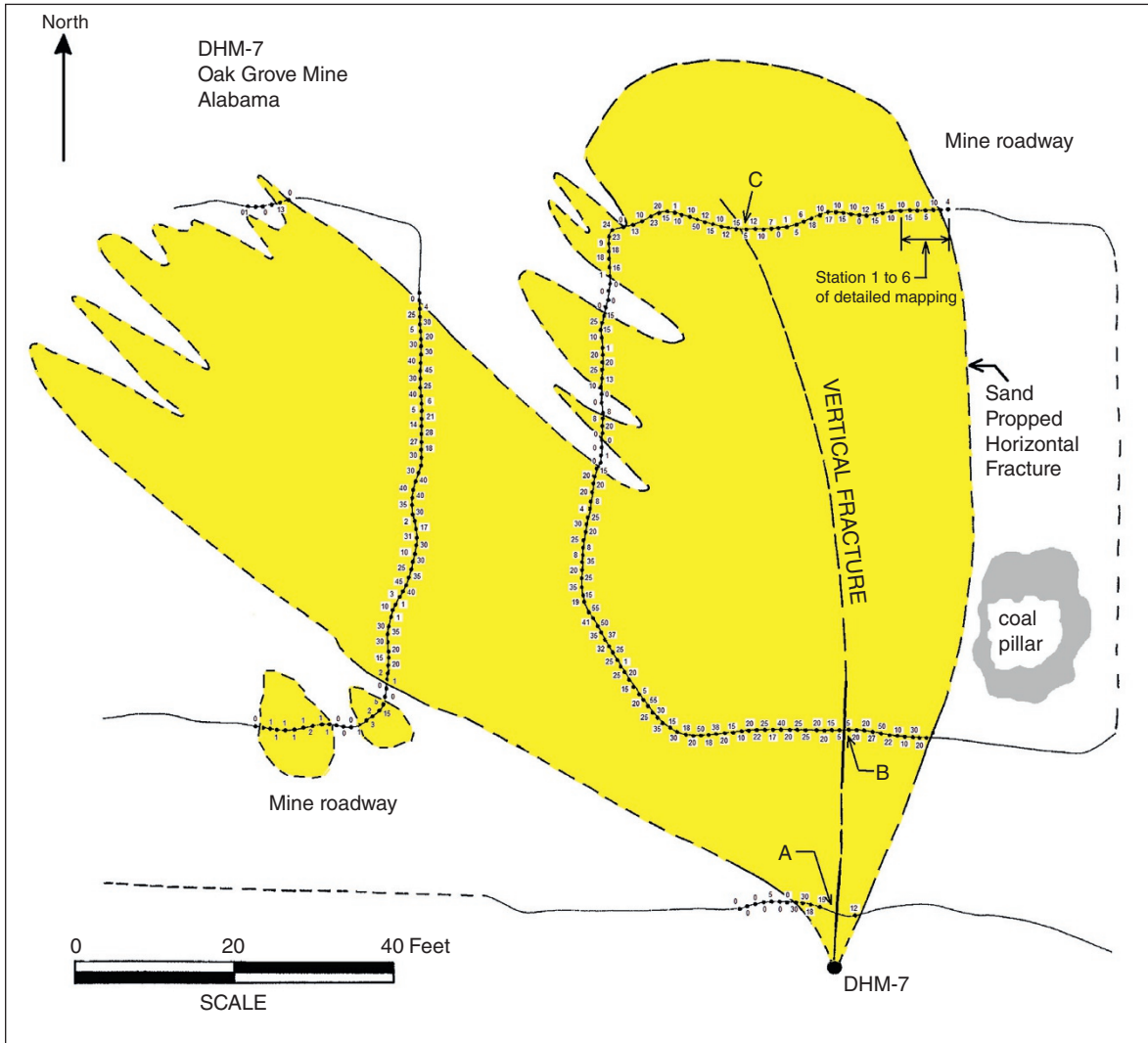
1.2.1.2 DDH 190 Fracture

An uncased HQ-size cored borehole (DDH 190) was drilled through the German Creek coal at Central Colliery in Queensland and was hydraulically fractured using a borate crosslinked hydroxypropyl guar gel fluid. The site was characterized by undertaking well testing, stress measurement, core testing, and fracture testing before the main fracture treatment. Table 1.2 summarizes the site parameters relevant to the treatment as given by Jeffrey et al. [5].

Mapping of the fracture during and after development of the roadways in this area of the mine revealed a vertical fracture in the coal that extended into the roof rock (Figure 1.3). The fracture trace in the roof rock (Figure 1.3a) was primarily a single fracture, but interactions with natural fractures resulted in the formation of some offsets and short parallel branches. The vertical fracture trace in the coal at the north side of 13 cut-through (Figure 1.3b) was typical of other vertical sections mapped at this site, consisting of a single fracture that interacted with bedded and sheared coal. The 150 mm-thick mid-seam shear zone (mssz) runs through much of the German Creek seam and is composed of sheared coal, with particles

Table 1.1 DHM-7. Coal, well, and treatment parameters.

Parameter	Value	Units	Description
σ_H	>8.1	MPa	Maximum horizontal stress
σ_h	6.2	MPa	Minimum horizontal stress
σ_v	8.1	MPa	Vertical stress
P_o	<3	MPa	Pore pressure (estimated)
k	1.2	md	Permeability, millidarcy
E	4000	MPa	Young's modulus of coal
ν	0.3		Poisson's ratio of coal
Q	0.022	m ³ /s	Injection rate
μ	25×10^{-9}	MPa s	Apparent fluid viscosity, at 170 s ⁻¹
Depth	331.3	m	Depth to top of Blue Creek seam
r	0.108	m	Wellbore radius



25 ● Mapping station with average sand thickness* for 1 foot section of horizontal fracture. * Sand thickness reported in hundredths of inches.

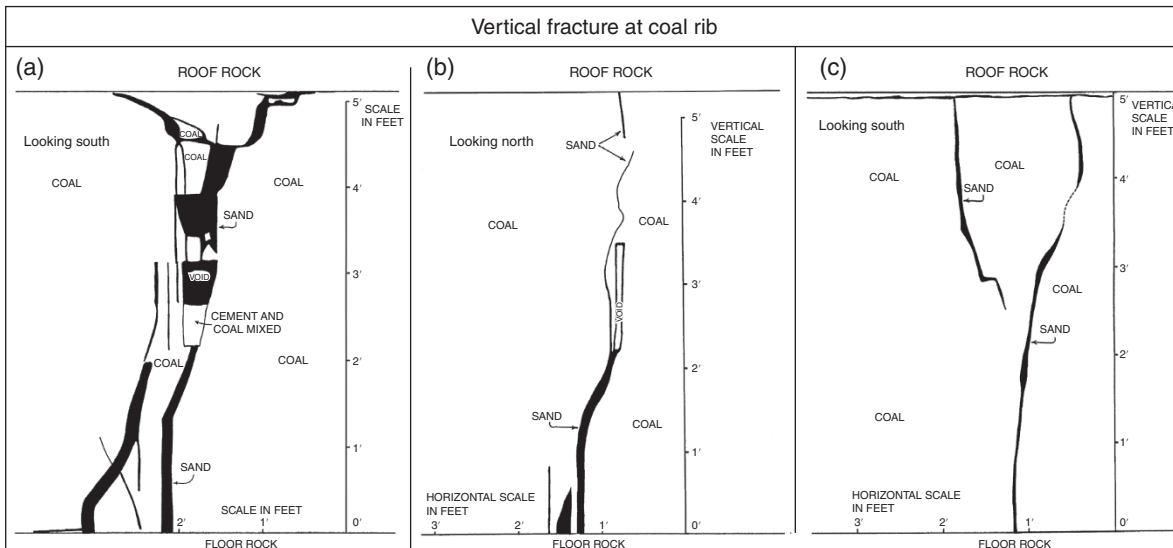


Figure 1.1 A plan view of the propped hydraulic fracture mapped at the DHM-7 site is shown in the top drawing while three mapped vertical fracture sections exposed at the coal rib are shown in the lower drawing. Mapping of the horizontal fracture occurred along the ribs of the roadways where the fracture was exposed near the roof (Source: Boyer et al. [12]/Gas Research Institute).

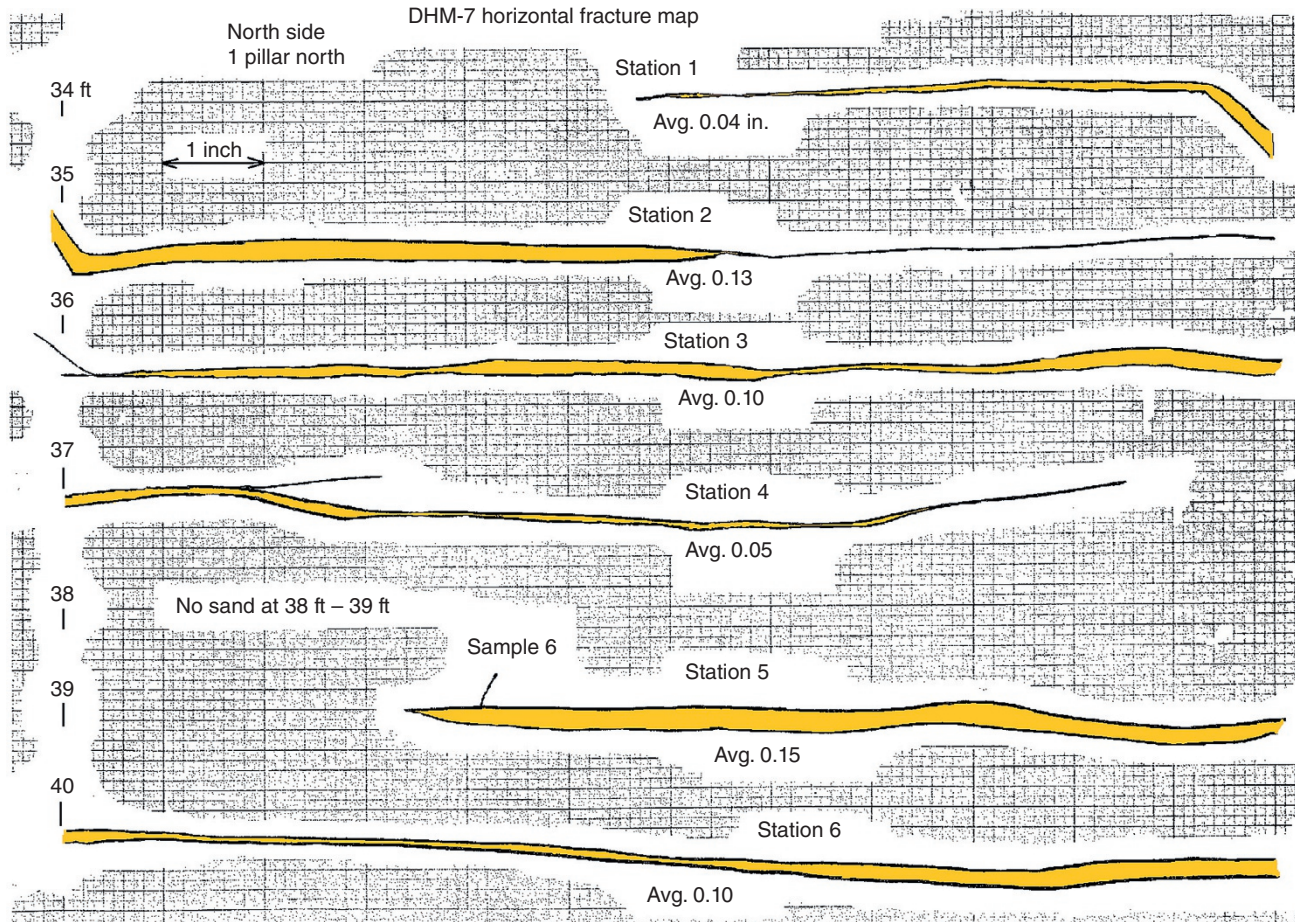


Figure 1.2 Seven linear feet of horizontal fracture mapped along the north side of the coal pillar (Source: Boyer et al. [12]/Gas Research Institute). The location of this portion of the horizontal fracture is indicated in Figure 1.1 and labeled as station 1 through 6. The entire horizontal fracture was mapped at this level of detail and the numbers in Figure 1.1 along the pillar boundary indicate the average propped width in hundredths of inches (e.g. 30 represents 0.30 in.).

Table 1.2 DDH 190 site parameters.

Parameter	Value	Units	Description
σ_H	>4	MPa	Max horizontal stress, in roof
σ_h	2.5	MPa	Min horizontal stress in coal
	1.9	MPa	Min horizontal stress in roof
σ_v	4.5	MPa	Vertical stress
P_o	1.08	MPa	Pore pressure
k	4.2	md	Permeability, millidarcy
E	2000	MPa	Young's modulus, coal
	25 000	MPa	Young's modulus, roof rock
ν	0.35		Poisson's ratio, coal
	0.13		Poisson's ratio, roof rock
Q	0.002 5	m ³ /s	Injection rate
μ	610×10^{-9}	MPa s	Apparent fluid viscosity at 170 s^{-1}
Depth	193.5	m	Depth to top of German Creek seam
r	0.048	m	Wellbore radius

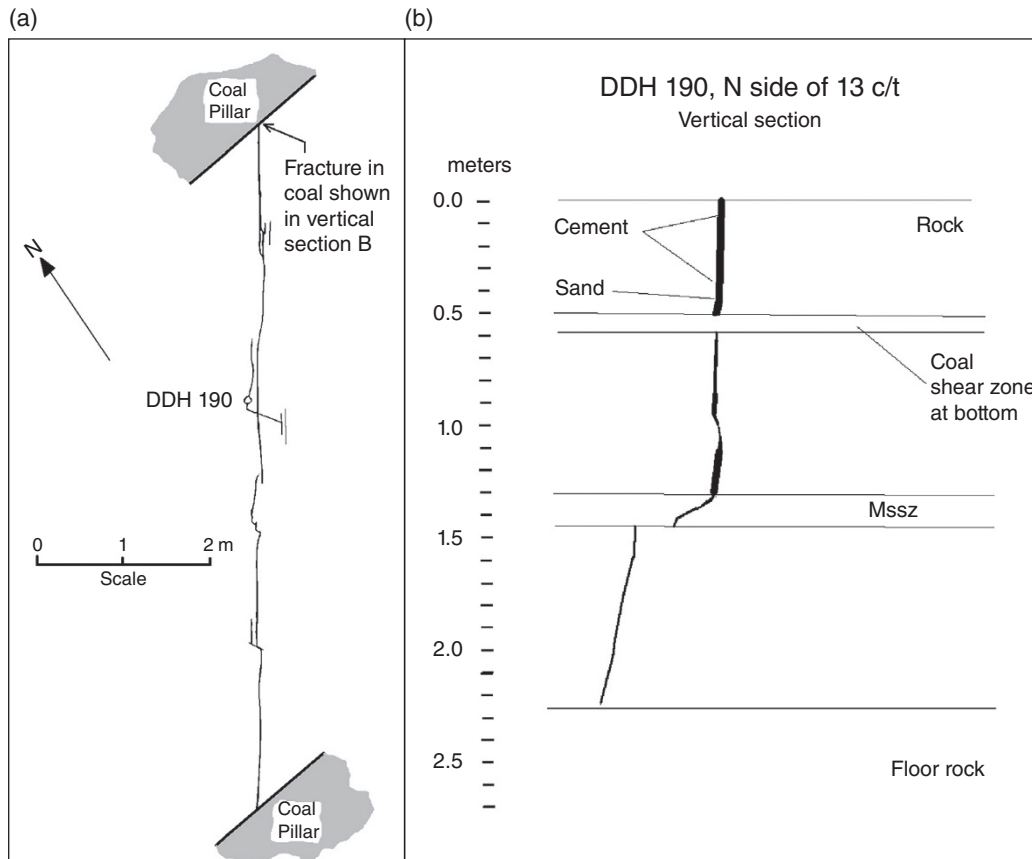


Figure 1.3 Looking down on propped fracture trace (a) in sandstone roof rock at 13 cut-through. Vertical section (b) showing propped fracture exposed on north coal rib of 13 cut-through near borehole DDH 190 (Source: Jeffrey et al. [5]/Coalbed Methane Association of Alabama).

ranging from clay size to a few centimeters in size. The mssz is softer and weaker than the coal above and below it. This hydraulic fracture and others mapped in this coal seam often developed an offset across the mssz.

The fracture at DDH 190 extended into the lower stress roof rock with only 12% of the proppant injected estimated to be accounted for by the propped fracture in the coal seam. The mapping clearly shows the trace of the propped hydraulic fracture in the roof and in the coal, but does not reveal if the fracture was growing primarily laterally or vertically at the sections mapped. Modeling of this fracture suggests upward growth of 7 m into the roof rock at the borehole [13].

1.2.2 Fractures in Hard Rock

Hydraulic fracturing is used in mining to induce caving and to precondition rock for caving [7]. More recently, preconditioning has been used in areas of high stress as a means of reducing the potential for the occurrence of large, damaging seismic events [14]. A total of nine fractures have been mined and mapped at four metalliferous mine sites in

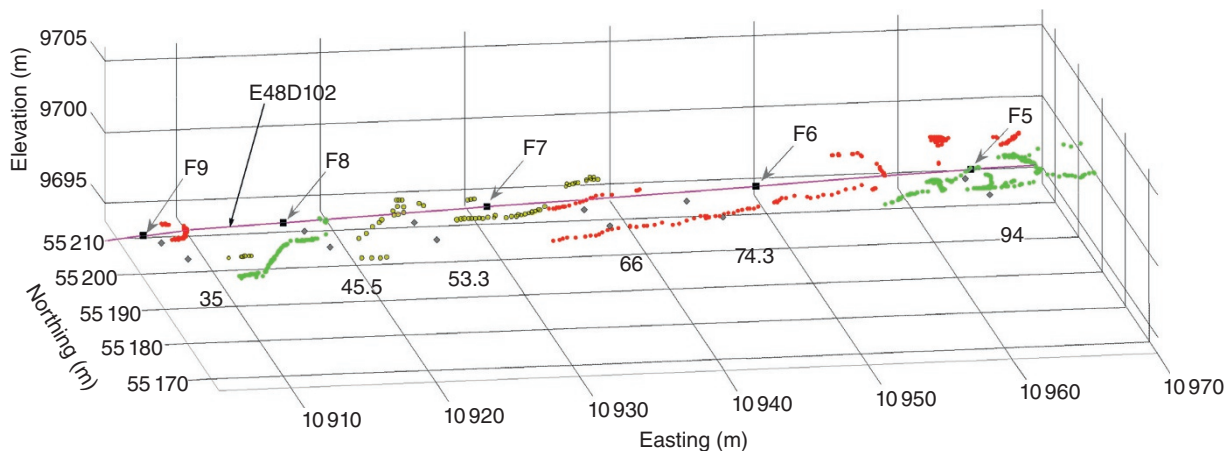
Australia [7, 9, 15] and Chile [6]. The fractures described by Jeffrey et al. [9] will be compared to the fractures placed into coal seams.

1.2.2.1 Northparkes E48 Mapped Fractures

Six hydraulic fractures were placed ahead of a tunnel at 580 m depth at the E48 Northparkes mine as part of a mine-through experiment [9]. The fractures were propped with colored plastic and sand and were monitored by microseismic and tiltmeter arrays. The mapped hydraulic fractures at Northparkes consist of nearly horizontal segments with offsets at intervals along them produced as the fracture grew into and along dipping veins, natural fractures, and shear zones. Fracture branches and sub-parallel propped sections were also mapped, making up 10–15% of the total fracture extent. The rock mass at the site is naturally fractured, containing approximately five natural fractures per meter. Additional details of the site, fracturing, and mine-back can be found in Jeffrey et al. [9]. Table 1.3 lists site and rock parameters. The stress directions given in Table 1.3 are based on overcoring data measured near the fracture site.

Table 1.3 Site and rock parameters for Northparkes E48.

Parameter	Value	Units	Description
σ_H	40	MPa	Max horizontal stress, 290 ^o , 8 ^o dip
σ_h	22	MPa	Min horizontal stress, 22 ^o , 11 ^o dip
σ_v	15	MPa	Vertical stress, 165 ^o , 76 ^o dip
P_o	<1	MPa	Pore pressure
k	0.005	md	Permeability, millidarcy
E	50 000	MPa	Young's modulus
ν	0.2		Poisson's ratio
Q	0.007 5	m ³ /s	Injection rate
μ	610 × 10 ⁻⁹	MPa s	Apparent crosslinked gel viscosity at 170 s ⁻¹
	1 × 10 ⁻⁹	MPa s	Viscosity of water
Depth	580	m	Depth below surface
r	0.048	m	Wellbore radius

**Figure 1.4** Hydraulic fractures mapped along a tunnel at the Northparkes E48 mine (Source: Jeffrey et al. [9]/Society of Petroleum Engineers). The initiation point of each fracture is indicated along the borehole which is drawn with a purple line.

The minimum stress was nearly vertical with the maximum stress oriented nearly horizontal and directed approximately east–west.

The hydraulic fractures were mapped along the E48D102 tunnel as it was driven. The fractures were horizontal with steps along their path often forming where they interacted with natural fractures and shear structures. These offsets were large enough to increase the average dip because the fracture trace following a stair-step pattern. Figure 1.4 shows an overview of the five fractures that were propped with colored plastic and mapped along the sides of the tunnel.

Fractures 6 and 7 were placed using crosslinked guar gel while fractures 5, 8, and 9 were placed using water. The colors of the points mapped along each fracture shown in Figure 1.4 correspond to the colors of the plastic proppant

used. The grid lines shown are the mine coordinates in meters. The initiation point of each fracture is indicated by a black square symbol and the borehole is shown by the line connecting these symbols. Figure 1.5 contains a more detailed sketch of Fracture 8, which contained the largest offset or step mapped in any of the fractures at this site. The injection interval, which was in the borehole E48D102, is shown. This interval is located approximately 2.5 m out of the plane of the fracture trace shown because the borehole was drilled along the centerline of the tunnel. Fracture growth is likely to have been semi-radial from the injection interval and should not be visualized as occurring purely along the fracture trace. Fracture 7 contained an offset similar in size to the one shown in Figure 1.5 and a series of smaller offsets (but consisting of 200–400 mm steps) were

- injection rate, DEM **166**, 166–168, 167–168, 172
- inlets, separate 184–185
- inlets, shared 183–184
- interaction 76–79, 77–78
 multiple clusters 79–81, 80–83
 zipper-stage injection 83, 83–84
- interference, fracture 75–85
 discrete fracture network (DFN) 75, 82, 82–83
 hydraulic fractures, fractured medium 81–83
 hydraulic fractures,
 interaction 76–79, 77–78
 hydraulic fractures, multiple clusters 79–81, 80–83
 hydraulic fractures, zipper-stage injection 83, 83–84
- natural fractures,
 interaction 76, 76–77
- numerical studies 75–83
- principal stress 79
- stress contours 78
- stress shadow effect 76, 81–82, 84
- XSite* code 75
- XSite* model 77, 77, 79, 82
- iteration loops, unstructured mesh 68
- intradyke spacing 202
- k**
- KGD model 227
- Kresse, complex fracture model 177–178, 178
- l**
- laminar flow 116, 119–122, 122
- lateral front splitting 181
- lattice model, fracture
 interference 75–85
 discrete fracture network 75, 82, 82–83
 hydraulic fractures, fractured medium 81–83
 hydraulic fractures,
 interaction 76–79, 77–78
 hydraulic fractures, multiple clusters 79–81, 80–83
 hydraulic fractures, zipper-stage injection 83, 83–84
- natural fractures,
 interaction 76, 76–77
- numerical studies 75–83
- principal stress 79
- stress contours 78
- stress shadow effect 76, 81–82, 84
- XSite* code 75
- XSite* model 77, 77, 79, 82
- layered formations 41–42, 42
- leak-off, dimensionless 136
- leak-off toughness 133–134
- leak-off viscosity 133
- LEFM, see linear elastic fracture mechanics
- LHFM, see linear hydraulic fracture mechanics
- linear elastic fracture mechanics (LEFM) 103, 127, 227
- linear hydraulic fracture mechanics 13
- linear inverse problem, tiltmeter 25–26
- m**
- Mackenzie Giant Dyke Swarm 193, 194, 196, 202
- mapped fracture geometries 7–8
- material inhomogeneity, DEM 172
- mathematical modeling 87–91, 88
- maximum principal stress 77–78, 157, 210, 256
- mesh, unstructured 65–74
 channel elements 66, 66–67
 crack surface remeshing 69
 discrete elasticity equation 66–67
 element remeshing 71–72, 72
 front update 68, 68
 iteration loops 68
 moving edge 68, 70, 73
 numerical simulations 70–72, 70
 planar hydraulic fracture 65–67
 simulation results 71, 71
 solution algorithm 69–70
 stress barriers 70–72, 70
 tessellation, triangular element 65, 73
 time-marching algorithm 67–70
 tip elements 66, 66–69
- microcrack-band 43
- microcracks, fracture tip 179–181, 180
- microseismicity 251
- microseismic monitoring 59–60, 59–60, 251–252
- mineback mapping 1–10
 coal fractures 1–5, **2**
 DDH 190 fractures 2–5, **4**, 5, 8
 DHM-7 fractures 2, **2**, 3, 8
- E48 Northparkes mine 5–8, **6**, **6**
- fracture geometry **8**
- hard rock fractures 5–7
- horizontal fractures 4
- mapped fracture geometries 7–8
- parameters,
 nondimensional 7–8, **7–8**
 resolution of observation **8**
 vertical fractures 3
- mined fractures, mapping 1–10
 coal fractures 1–5, **2**
 DDH 190 fractures 2–5, **4**, 5, 8
 DHM-7 fractures 2, **2**, 3, 8
 E48 Northparkes mine 5–8, **6**, **6**
 fracture geometry **8**
 hard rock fractures 5–7
 horizontal fractures 4
 mapped fracture geometries 7–8
 parameters,
 nondimensional 7–8, **7–8**
 resolution of observation **8**
 vertical fractures 3
- mixed-mechanism
 stimulation (MMS) 44
- mkc*-asymptote 95
- mk*-scaling 118–119
- moving edge, unstructured mesh 68, 70, 73
- moving element mesh,
 unstructured 65–74
 channel elements 66, 66–67
 crack surface remeshing 69
 discrete elasticity equation 66–67
 element remeshing 71–72, 72
 front update 68, 68
 iteration loops 68
 moving edge 68, 70, 73
 numerical simulations 70–72, 70
 planar hydraulic fracture 65–67
 simulation results 71, 71
 solution algorithm 69–70
 stress barriers 70–72, 70
 tessellation, triangular element 65, 73
 time-marching algorithm 67–70
 tip elements 66, 66–69
 unstructured mesh 66, 73
- MPS, see maximum principal stress
- multi-cluster fractures 226, 229, 233–235
- multiple clusters, hydraulic fractures 79–81, 80–83

- multiple fractures 241–243, 242
m-vertex solution 95
- n**
- natural fractures 1, 40–41, 40–41
 DEM modeling 142–153, **144**, 144, 147, 155, 171
 fraction swarms, front
 branching 181–182
 interaction 76, 76–77
 intersections 151–153, 152–153, 172
 nonlinear fracturing 42–43, 43
 non-orthogonal crossing 150–151, 151
 nonplanar fault 256
 nonzero leak-off 121–122
- o**
- ODE, *see* ordinary differential equation
 offset crossing, DEM 148
 oil and gas reservoirs 38–43
 operational parameters **235**, 235–236
 ordinary differential
 equation (ODE) 90
 orthogonal crossing 145–146, 146, 148, 172
 orthogonal natural fractures 145–146, 146–147
- p**
- parallel fractures 182–185, 184, 188
 parameters
 nondimensional 7–8, 7–8, 246
 operational **235**, 235–236
 parametric space 119–122, 122–123, 130, 135
 particle flow code, *see* PFC
 perforation diameter 245
 Perkins–Kern–Nordgren, *see* PKN
 fracture geometry
 perspective view, fracture swarms 179
 PFC 143–145, 143–144, **144**, 147–149, 149–150
 PFC2D 141
 PKN fracture geometry 107, 128–130, 130, 134–136; *see also*
 planar fault 256
 planar fractures 91–92, 102
 planar fractures, unstructured
 mesh 65–67
 plane strain 127
 plasticity 99–105
 brittleness index 102–103, 103
 closure stress 101–102
 fracture containment 102–103
 fracture toughness **101**, 101–102
 linear elastic fracture mechanics
 (LEFM) 103
 planar fractures 102
 propagation direction 100–101, 100
 PNM, *see* pore network model
 point-load hydraulic fracture 16–17
 point source dislocation singularity
 model, tiltmeter 28–29
 point source forward model,
 tiltmeter 31, 32
 pore network model 141–142, 142, 166, 171
 porosity **12**
 Prandtl–Karman coordinates 110, 111
 pressure, DEM modeling 158–160, 159–161, 168
 principal stress (PS) 78, 79
 process zone 45
 production temperature 214–216, 215
 propagation, thermal fracturing 210, 210, 216–221
 propagation conditions 88–89
 propagation direction 100–101, 100, 110–112, 229
 propagation regimes 115–118
 proppants carrying, scCO₂
 fracturing 59–60
 PS, *see* principal stress
- q**
- quakes, *see* seismic events
- r**
- radial hydraulic fracture **14**, 107–126
 boundary conditions 110
 crack elasticity equation 109
 field applications 112–115
 fluid flow 109–110
 fluid-volume balance 110–111
 fracture propagation 110–112
 friction factor 111
 laminar flow 116, 119–122, 122
mk-scaling 118–119
 nonzero leak-off 121–122
 parametric space 119–122, 122–123
 PKN fracture geometry 107
 Prandtl–Karman
 coordinates 110, 111
 propagation regimes 115–118
 Reynolds number 107–111, 111
 spatial variations 109, 113–116
 turbulent flow 108
 turbulent-laminar flow 113–114, **115**, 119–122, 121, 123–124
 zero leak-off 120–121
 radiography scans, scCO₂ fracturing 56
 resolution of observation **8**
 Reynolds number 107–111, 111
 rock, intact, DEM 144–145, 157–159, 172
 rock deformation 209–210
 rock properties **12**
- S**
- sandstone 1
 SC-CO₂, DEM 158–159, 172
 scCO₂ fracturing 51–64
 challenges 60–61
 CO₂ phase 61
 equipment, specialized 61
 experiments 54–57
 field test, first 58, 57–60
 fracture geometry 59–60, 59–60
 fracturing process 58, 58–59
 fracture tortuosity 56
 macroscale mechanical
 changes 53–54
 microscale chemical changes 52–53
 microscale mechanical changes 52
 microseismic
 monitoring 59–60, 59–60
 numerical simulations 57
 operation parameters 58–59
 products data 60
 proppants carrying 59–60
 radiography scans 56
 SEM images 52
 shale 52–54, **53**
 simulations 60
 technology 57–58
 triaxial loading 54, 54–57
 Yan-A well fractures 59
 Yan-B well fractures 60
 Yanchang oil field 57–60
 SCR viscous asymptote 87
 seam gas 1
 seismic events 251–261
 boundary conditions 253–254
 closed fractures 254–256
 elastodynamic models 259
 fault permeability 254–256
 energy, radiated 256–258
 fluid front 253–254
 Green's function 208, 253
 injection-induced 251–252, 252

- open fractures 256
 - nonplanar fault 256
 - planar fault 256
 - microseismicity 251
 - microseismic monitoring 251–252
 - modeling 252–256
 - strength, frictional 258
 - stress, shear 258–259
 - SEM images, scCO₂ fracturing 52
 - semi-infinite crack 89–90
 - shale reservoirs 177
 - shale, scCO₂ fracturing 52–54, 53
 - shear stress 258–259
 - simulator models, dyke swarms 203
 - situ stress 25
 - solid deformation 228–229
 - spacing, dominant, dyke swarms 202
 - spacing, fracture 239–240
 - spatial variations 109, 113–116
 - spatio-temporal evolution 11
 - spiral perforations, multiple fractures 179
 - stiffness contrast, DEM 149–150, 150, 172
 - storage toughness 133
 - storage viscosity 132
 - strains 27
 - strain monitoring 42, 43, 45
 - strength contrast, DEM 147–149, 172
 - strength, frictional 258
 - stress barriers
 - symmetric 95, 96
 - unstructured mesh 70–72, 70
 - stress closure 101–102
 - stress contours 78
 - stress drop 95, 96
 - stress field 209
 - stress plugs, dyke swarms 199
 - stress ratio, DEM 145–147
 - stress shadow effect 76, 81–82, 84, 197–198, 198, 245
 - stress, shear 258–259
 - strike-slip 26
 - surfaces, hydraulic fracture 18–19
 - swarming behavior 193
 - symmetric stress barrier 95, 96
- t**
- temperature distribution 216, 216–218
 - temperature, rock 213–214, 216, 216–218
 - tessellation, triangular element 65, 73
 - theory of solid mechanics 209
 - thermal fracturing 207–223
 - ABAQUS 208–209, 212–213, 221
 - ANSYS 207
 - boundaries 211
 - boundary element method (BEM) 208
 - COMSOL Multiphysics 207
 - coupled fluid-thermal solver 213–214, 214
 - degrees of freedom (DOF) 213
 - displacement discontinuity method (DDM) 208
 - displacement discontinuity vector 209
 - elastic traction–separation model 209
 - enhanced geothermal system (EGS) 207–208, 214–221
 - extended finite element method (XFEM) 208, 211–213, 216, 216–220
 - FEM discretization 211–212
 - finite difference method (FDM) 207
 - finite element method (FEM) 207–208, 211–212
 - finite volume method (FVM) 207
 - fluid flow 209, 211, 214–216, 215
 - fluid velocity 215
 - Fourier’s law 211
 - fracture, double 220–221, 220–221
 - fracture, single 216–220, 218–220
 - fracture-thermal model 211
 - geothermal energy 207
 - heat transfer 211, 221
 - Heaviside step function 212–213
 - Hooke’s tensor 209
 - mathematical model 208–209, 209
 - maximum principal stress (MPS) 210
 - production
 - temperature 214–216, 215
 - propagation 210, 210, 216–221
 - rock deformation 209–210
 - stress field 209
 - temperature distribution 216, 216–218
 - temperature, rock 213–214, 216, 216–218
 - theory of solid mechanics 209
 - thermal transport 211
 - thermoelastic model 207, 209–214
 - TOUGH2 code 207
 - XFEM discretization 212–213
 - thermal transport 211
 - thermoelastic model 207, 209–214
 - tiltmeter monitoring 25–36
 - Bayesian inversion method 30–31
 - dip-slip 26
 - displacement discontinuity vector 26
 - displacements 27
 - eigenstrain 26–30, 34
 - field applications 31–34
 - field tilt data 25
 - forward fracture model 25–30
 - fracture plane orientation 26
 - general distributed dislocation model 29–30
 - general planar forward model 31–34, 33
 - linear inverse problem 25–26
 - point source dislocation singularity model 28–29
 - point source forward model 31, 32
 - strains 27
 - strike-slip 26
 - tilts 27
 - Volterra dislocation 26
 - tilts 27
 - time discretization 231
 - time evolution 15–18
 - time-marching algorithm, unstructured mesh 67–70
 - time scaling, DEM 168–170, 169–170
 - tip asymptotics 87–98
 - boundary conditions governing equation 88–89
 - coalescent fluid 89
 - discretization 91–92
 - displacement discontinuity 91–92
 - elasticity 88
 - elastic medium governing equation 88
 - fluid flow governing equation 88
 - fluid and fracture front lag 88–89
 - fluid transport 88
 - fracture fronts 88–89
 - free boundary 92–93
 - governing equation 89–91
 - ILSA steps 92, 92–95
 - implicit level set algorithm (ILSA) 92–95
 - mathematical model 87–91, 88
 - mkc*-asymptote 95